ADVANCED ENGINEERING MATERIALS
www.aem-journal.com

Exploiting Structural Instability to Design Architected Materials Having Essentially Nonlinear Stiffness

*Jonathan Bunyan and Sameh Tawfick**

Architected materials enable unusual mechanical behavior, that is, inaccessible to existing materials. This study demonstrates an architected cell structure having a constant stress plateau extending for a very wide range of strains followed by hardening at large strains. This essentially nonlinear stiffness has attractive applications ranging from static stress redistribution to acoustic wave tailoring, yet materials exhibiting this behavior are challenging to realize practically. The authors propose designs which realize controlled essentially nonlinear response using coordinated elastic strut buckling. The authors exploit controlled asymmetric buckling of the struts' structure to precisely tailor a wide flat stress plateau in elastomeric materials. The authors experimentally measure the effects of structural geometry and provide design guidelines to tune this exotic behavior. The authors utilize finite element simulations to isolate the core strain energy storage mechanisms governing the deformation. Owing to the 2D nature of the design, these materials can be readily fabricated in a variety of materials using laser cutting, extrusion, molding, 3D printing, and micro-lithographic methods. The proposed designs have wider constant stress plateaus than open cell foams, and as such offer new opportunities in orthopedic design, protection, packaging, as well as sonic vacua and non-reciprocal acoustic metamaterials.

Elastic metamaterials can be engineered to achieve unusual mechanical properties derived from their underlying structural architecture. Such properties include auxetic materials,[1,2] materials with vanishing shear modulus,[3,4] and vanishing speed of sound.[5,6] The clever use of controlled buckling can be exploited to achieve these behaviors as well as tailor them to specific applications. For example, energy-absorbing materials use novel geometries to produce buckling behavior characterized by large negative stiffness[7] and bistability which make them suitable for energy trapping.[8] Programmable metamaterials exploit elastic instability to create state switching and shape memory effects[9,10] as well as acoustic metamaterials with switchable band structures.[11] In addition to negative stiffness and bistability, buckling behavior is also used to create broad regimes of zero stiffness behavior known as quasi zero stiffness (QZS). QZS vibration isolators can attenuate a wide range of external disturbances over a broad range of frequencies. Such isolators are achieved through the introduction of negative stiffness spring elements through pre-compression of buckling elements[12–15] as well as magnetic springs tuned to eliminate positive stiffness terms.[16,17] This behavior, in which the linear stiffness component is vanishingly small, is referred to as essentially nonlinear. It is an extremely attractive strain response which can create unusual dynamic behavior for wave propagation including the breaking of acoustic reciprocity.[18,19] Essentially nonlinear stiffness oscillators have a "natural frequency" which is tunable with energy, and as such have many applications in vibrations due to their ability to passively tune themselves in an internal resonance with the surrounding system.[20–22] One such example is the cochlea within the ear which uses essential nonlinearity to achieve compression of dynamic range, sharp tuning for quieter sounds and generation of combination tones.[23]

We report a class of 2D architected materials exhibiting essentially nonlinear stiffness: a flat-stress plateau followed by a hardening behavior. The architected material consists of elastic strut elements undergoing coordinated asymmetric buckling leading to a wide stress plateau followed by nonlinear stiffness increase. Two different structural architectures that exhibit qualitatively similar behaviors are investigated (See **Figure 1**). The first architecture consists of two struts fixed on a base forming a triangle. The essentially nonlinear force–displacement is probed by clamping the base of the triangle and applying a force on the apex. The force can be applied by an indenting flat surface which is brought into contact with the apex of the triangle (Figure 1). Though this structure resembles a von Mises truss,[24] its behavior is fundamentally different because of its boundary conditions. We refer to it as τ-spring (pronounced tau spring) due to its shape in the post-buckling regime. The second architecture consists of two mirrored τ-springs joined at the apex. The bridge connecting the apexes of the two triangles must restrict the struts on the two halves from rotating with respect to each other. This bridge hence needs to be sufficiently thick with respect to the strut widths. We refer to the second design as χ-spring (pronounced chi spring) due to its resemblance to the Greek letter χ. Both ends of the χ-spring

Prof. S. Tawfick, J. Bunyan
University of Illinois Urbana-Champaign
1206 W. Green St., Urbana, IL 61801, USA
E-mail: tawfick@illinois.edu

The ORCID identification number(s) for the author(s) of this article can be found under https://doi.org/10.1002/adem.201800791.

DOI: 10.1002/adem.201800791

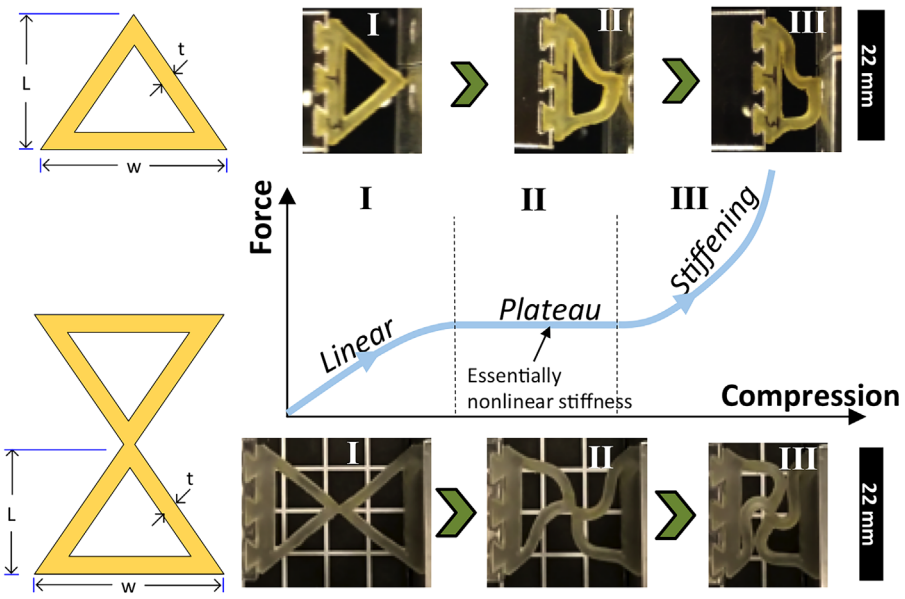

Figure 1. 2D Elastic elements: τ-spring (top) and χ-spring (bottom) with characteristic force–displacement behavior under compression showing three different regimes of behavior. Snapshots depict typical deformed states of the elements during each regime.

element are clamped and there is no sliding contact between the indenter and the element. As will be described in the manuscript, there are some similarities and differences between the behavior of the τ- and χ-springs. The force–displacement response of both the τ-spring and χ-spring can be divided into three regimes (Figure 1). Regime I is approximately linear and dominated by local compression of the material at the apex, axial compression of the struts, or symmetric buckling modes.

Following the linear regime, transition to the flat stress plateau regime takes place as the struts buckle asymmetrically (regime II in Figure 1). The zero-stiffness regime is extremely interesting. As discussed in the introduction, several applications would benefit from such zero stiffness regime in static load redistributions as well as acoustic wave tailoring. The flatness and repeatability of the zero stiffness regime motivated the study of the dependence of the features of this regime, such as the plateau width, on the internal structural architecture.

Regime III starts when structural elements, which are initially separate from each other, severely deform until new solid–solid contact regions are created (densification). When new contacts are formed, a nonlinear stiffening behavior is observed. In the case of the τ-spring the new contact points arise between the strut elements and the indenting surface, as well as between the strut elements themselves. In the case of the χ- spring the contact points are only between strut elements. The combination of regimes II and III constitute the essentially nonlinear behavior which can be precisely tailored by the internal structural geometry. Interestingly, similar three-regime behavior has historically been observed in the compression of many foams —disordered or honeycomb, elastic or plastic, open cell or closed cells.[25–27] However, it is difficult to precisely control the slope of the stress "plateau" in traditional foams. In the densification regime III, the stress increases more steeply with strain, which can be attributed to new contacts among the various cells. These contacts cause hysteresis in foams, and vary with repeated compression cycles.

Both structural architectures exhibit extremely flat force plateau, which make them very attractive for a variety of uses. The χ-springs offer wider stress plateau than τ-springs. This is especially apparent in regime II and III and is depicted in **Figure 2**a and **3**a. Understanding and tailoring the plateau width and the subsequent stiffening is especially useful in acoustic metamaterials. For example, if χ-springs are arranged in a pre-compressed state, their ideal flat plateau region II followed by the stiffening regime IIs will behave similarly to a vibro-impacting system. The later has many applications in wave tailoring but suffers from noise and construction complexity. In this study we are particularly interested in the essentially nonlinear behavior of regime II. It is possible to achieve weak negative stiffness in regime II, however, this does not necessarily result in bistability of the element since it occurs at sufficiently large pre-compressions and the applied load does not change direction (remains in pre-compression).

τ- and χ-springs are fabricated by cutting a 3/16 inch-thick sheet of polyurethane rubber (Abrasion-Resistant Polyurethane Rubber 60A) using a laser cutter (Epilog Mini 18). These samples are designed with a puzzle-piece geometry at the base to facilitate easy sample replacements on the test setup. A custom built mechanical testing device is used for testing. Data collection and control of the test setup (pictured in the Supporting Information) is done using NI DAQ input modules connected to a Futek LSB200 10lb loadcell while actuation of the sample is done through Thorlabs LNR50S stepper motor controlled through a BSC201 controller. Samples are subject to compression and each sample is cyclically loaded and unloaded several times to eliminate initial hysteresis, as is commonly done in testing elastomeric materials. Following five cycles, the response is repeatable. The force–displacement relationship for a τ-spring

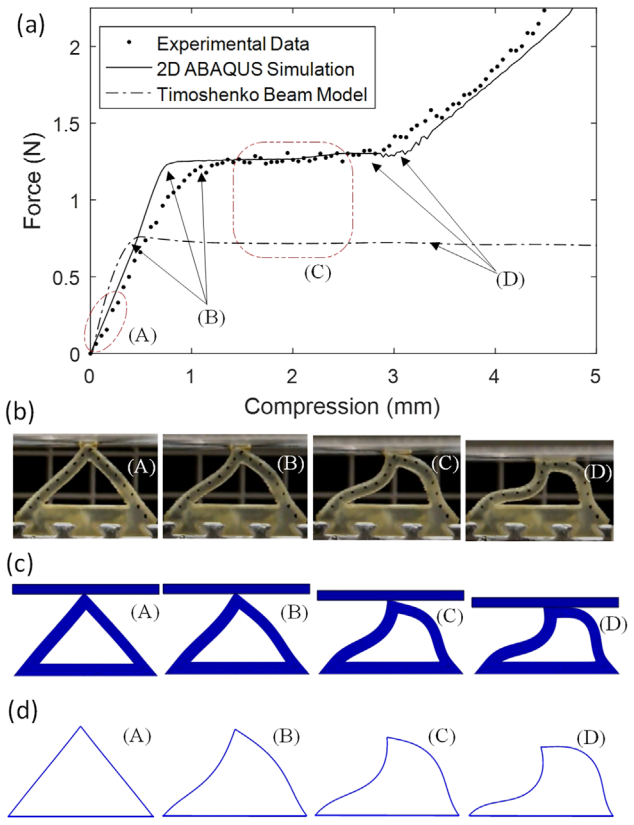

Figure 2. Force–displacement relationship for τ-spring. a) Experimental data plotted against simulated response using various models; b–d) snap shots of the deformed state of the τ-spring with $t = 1.72$ mm, $L = 14$ mm, $w = 22$ mm at various points of interest along the force–displacement curve for the experiment, c) 2D finite element model, and d) Timoshenko beam finite element model.

sample with measured width, length and thickness of 22, 14, and 1.72 mm, respectively, is depicted in Figure 2a. Snap shots of the deformed element at the beginning of regime I (A), the transition to regime II (B), the middle of regime II (C), and the transition to regime III (D) are depicted in Figure 2b. This design robustly demonstrates essential nonlinear behavior. Depending on the application, the τ- and χ-springs can be used as individual spring elements, or repeated to construct periodic lattice materials. The photos associated with each regime in the force–displacement response depict the mechanism responsible for the behavior.

Essentially nonlinear stiffness is observed when the local stress state leads to perfect stiffness cancelation. To better understand the local stress state leading to essentially nonlinear behavior, we use four-node bilinear 2D plane stress elements created in the commercial finite element analysis (FEA) software ABAQUS. A small perturbation is applied to the apex of the elements in the FEA model to promote buckling into the asymmetric mode. First, we discuss the material constitutive law used in the numerical simulation of the springs. We conduct tensile tests of the polyurethane rubber and find that it is best described by a Mooney-Rivlin constitutive law with $C_{01} = 0.29$ MPa and $C_{10} = 0.35$ MPa (see Supporting Information). Further details of the FEA simulation can be found in the Supporting Information. Using these parameters in explicit FEA, the simulation result agrees with the experimental measurement very well capturing the initial linear regime I, the plateau regime II and the hardening regime III (Figure 2, 3). This agreement with FEA is extremely promising as it indicates that the flat plateau indeed results from the internal architecture, and not from uncontrolled experimental factors. The ability to capture the behavior in explicit FEA simulations using commercial FEA software indicates the possibility to predictively design these architected materials and tailor them for specific device applications. We note minor deviation between the experiments and FEA near the transition to the asymmetric buckling mode (regime I to regime II transition), as well as minor delays of the onset of hardening in the simulations (transition from regime II to III). These transitions appear to be sensitive to defects in fabrication and assembly such as

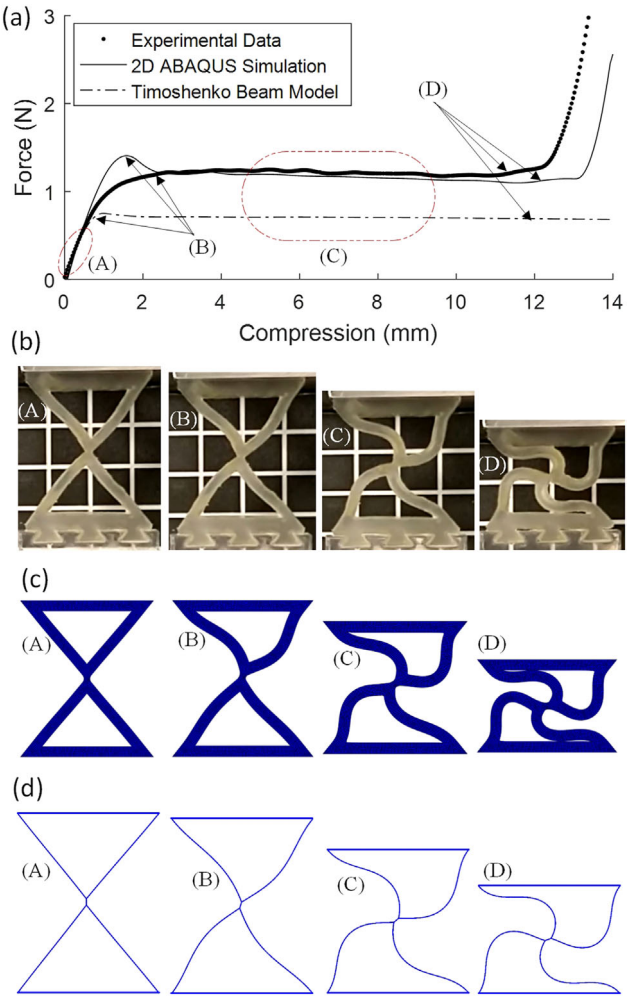

Figure 3. Force–displacement relationship for χ-spring. a) Experimental data plotted against simulated response using various models; b–d) snap shots of the deformed state of the χ-spring with $t = 1.72$ mm, $L = 14$ mm, $w = 22$ mm at various points of interest along the force–displacement curve for the experiment, c) 2D finite element model, and d) Timoshenko beam finite element model.

out-of-plane tapering and other minor defects including non-rectangular cross sections. We observe that, a linear constitutive law produces nearly identical results to the hyperelastic model and thus conclude that it is reasonable to use a linearized constitutive law with $E = 3.84$ MPa and $\nu = 0.4$ (see Supporting Information). This also indicates that the behavior arises solely from the architecture, and hence can be agnostic to material selection. This can open opportunities in fabricating these springs for a wide range of materials, as long as their aspect ratio ensures they do not break.

We further analyze the behavior of the springs to understand the elimination of stiffness within the plateau, leading to this unusual load–displacement behavior. In particular, we investigate the role of bending strain energy in governing the constant load plateau. Moreover, a bending energy dominated behavior would indicate the suitability of a wide range of non-elastomeric materials to obtain this behavior, and open tremendous design opportunities for hard polymers (e.g., nylon, polyethylene) and metallic structures. On the other hand, a large compression/tension strain dominated response would indicate the need for elastomeric struts to obtain essentially nonlinear stiffness. By applying a Kraty-Porod model[28] to the centroid nodes from the 2D plane stress FEA solution we conclude that the flat stress plateau is governed solely by bending strains in the struts. This analysis is discussed in detail in the supplementary information. We note that both bending and compression/tension govern the linear behavior in regime I.

Based on this insight, we propose a Timoshenko beam model to simulate the behavior of springs within regime II using ABAQUS. The accuracy of beam element simulations in capturing the flat plateau can open opportunities to designing similar architected materials from thin slender metal elements. In these simulations, the struts, which use ABAQUS 2D beams elements, are subject to encastre (clamped) boundary conditions at the base and a tie constraint at apex, that is, no relative displacement or rotation between struts at the apex. The cross-section of the beam elements corresponds to the geometries used in the experiments, and the linear elastic material constitutive properties described previously are used. Deformation is applied by a vertical displacement boundary condition on the apex. The resulting force–displacement curve is depicted in Figure 2 and snap-shots of the deformed element are depicted in Figure 2d. The beam initially deforms in symmetrical buckling mode resulting in a linear behavior that does not coincide with the experimental data over regime I since it is caused by a different mechanism. Following an initial linear response, a flat zero-stiffness plateau is obtained. Hence, the Timoshenko beam model FEA predicts the behavior in regime II. Notably, the transition from regime I to II using the Timoshenko model takes place earlier than in the experiments or the other FEA approaches. We attribute this premature transition to the fundamental differences in regime I between the 2D model and experiment which includes local compression as well as symmetric buckling and the Timoshenko model which only captures symmetric buckling. This causes the Timoshenko model to rapidly "snap" into the asymmetric buckling behavior (regime II) instead of smoothly transitioning into it. Notably, the linear regime and transition into the asymmetric buckling mode is shown, in this case, to play an important role in the amount of energy that can be stored by the element over regime I and regime II. Specifically, by delaying the onset of regime II, more energy can be stored over a compression spanning regime I and II. The plateau persists over the entire compression range as the stiffening behavior (regime III) is not captured due to the absence of contact interactions.

Next we study the mechanical behavior of the χ-spring. The force–displacement relationship for a polyurethane rubber spring having width, length and thickness of 22, 14, and 1.72 mm, respectively, is depicted in **Figure 3**a and snap shots of the deformed element at the beginning of regime I (A), the transition to regime II (B), the middle of regime II (C), and the transition to regime III (D) are depicted in Figure 3b. The force–displacement behavior is very similar to that of the τ-spring. However, the plateau region (regime II) is more than three times wider −persisting to larger deformations- and the stiffening behavior (regime III) is much more pronounced. Unlike the τ-spring, additional points of contact are not initiated at the apex but between the struts and base at much larger compressions. The plateau region is extended due to the absence of new contact points initiating at the apex-indenter interface. Initiation of contact occurs at two regions almost simultaneously, at the top and bottom base, and the deformed structure is much closer to densification at the onset of the stiffening behavior (regime III).

FEA is used to simulate the behavior of the χ-springs. One end of the χ-spring element is clamped and the other is subject to a displacement boundary condition. Additional information about the simulation can be found in the Supporting Information. The simulation agrees very well with the experimental results, particularly capturing the behavior within each regime. The transitions from regimes I to II and from II to III show deviation from the experimental measurement. Similarly, we use a Timoshenko beam model in FEA with the one base subject to an encastre boundary condition while the other is subject to a vertical displacement boundary condition. As in the case of the τ-spring, the Timoshenko model captures the zero-stiffness plateau behavior.

To our knowledge, even though the stress plateau is regularly reported in the cellular materials literature, the behavior within the stress plateau has not been systematically studied due to lack of control on stress localization in a multi-cell honeycomb structure. In all the discussed cases, we describe regime II as a zero-stiffness plateau. When the internal structural architecture is varied, for example, by changing the width of the struts, the stiffness can deviate from this ideal behavior demonstrating slightly positive or negative load–displacement slope. We define metrics to analyze the features of the stress plateau. The behavior of the essentially nonlinear material can be described by the average stiffness in the plateau region, the width of the plateau, and the energy stored within regimes I and II before the stiffening. An experimental parametric study is conducted to probe the range of tunability of the essentially nonlinear response of the τ- and χ-springs. Specifically, the struts' thickness is varied in the range $1.5\,\text{mm} \leq t \leq 2.5\,\text{mm}$ and the struts' length is varied in the range $10\,\text{mm} \leq L \leq 18\,\text{mm}$ in increments of 0.25 and 2 mm, respectively. Results for both the τ- and χ-springs are depicted in **Figure 4**a and b, respectively.

First, we consider average plateau stiffness defined as the slope of the line of best fit over the plateau (regime II). The closer

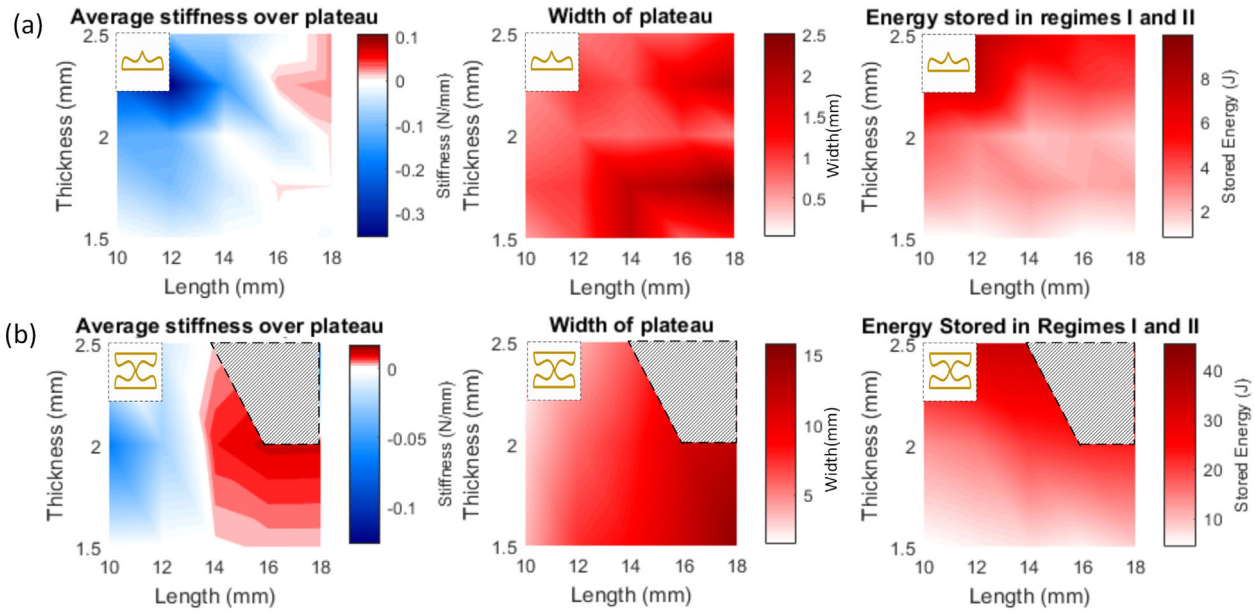

Figure 4. Tailoring architected metamaterials. Parametric study of the effects of geometry on the average stiffness over regime II (left plots), width of regime II (middle plots) and the energy stored in the elements over regime I and II (right plot) for the a) τ-spring and b) χ-spring. Hatched regions in b) indicate parameters over which the samples buckled out of plane. Regions with inset schematic depict the symmetrical buckling shape of the τ- and χ-springs within the dashed line-outlined geometries.

the average plateau stiffness approaches zero, the closer the spring is to the ideal behavior within the essentially nonlinear regime II. In the case of the τ-springs, the plateaus remain relatively flat compared to the linear stiffness O(1 N/mm) with in the range of $L > 14$ mm and $t < 2$ mm. In the case of the χ-springs, the plateaus are almost flat, corresponding to nearly ideal zero-linear stiffness compared to the regime I linear stiffness O(1 N mm^{-1}) over the range of parameters tested. χ-springs with $L < 14$ mm exhibit weak negative stiffness over the plateau while samples with $L > 14$ mm exhibit weak positive stiffness over the plateau. While for the τ-springs, there is no clear trend between positive and negative average plateau stiffness over the range of geometrical parameters tested. When L is very long with respect to the base width (large aspect ratio), χ-springs buckled out of plane and were not included in the study (hatched region in Figure 4b). The τ- and χ-springs with $L = 10$ mm and $t = 2.5$ mm (having very short aspect ratio struts) do not buckle asymmetrically and are excluded.

Next, we present the study of the width of the zero-stiffness plateaus. τ- and χ-springs having thinner, taller struts exhibit wider plateaus. Plateau width extends the range of strains of the architected material before stiffening and densification (regime III) occur. The ability to tune the width of the plateau is a useful design attribute of these springs.

The final attribute of the τ- and χ-springs is the amount of energy stored over regimes I and II. The energy stored is computed as the area under the force–displacement curve and parametrically plotted in Figure 4a and b. For both springs, struts with thicker width tend to store the most energy as they tend to persist in regime I for longer and require greater force to buckle asymmetrically into regime II— plateaus occur at a larger compressive force.

To demonstrate the tailorability and robustness of these architectures we examine their performance in applications of materials having essential nonlinearity in distributing static mechanical stresses. Possible applications include cushioning, packaging or orthopedics. Stress re-distribution can for example minimize bedsores (pressure ulcers) in addition to offering comfort. For example, state-of-the-art commercial foams are made from low density materials which exhibit a plateau stress response. The plateau response is typically preceded by a linear slope similar to regime I for the lattices presented in this study. The transition from regime I to II usually involves a peak stress, followed by negative stiffness associated with the foam buckling, then followed by a stress drop to the stress plateau level. Materials having this kind of general response, exhibiting a stress plateau are used for cushioning as they accommodate the non-uniform geometry of a contacting hard surface by local buckling and distribution of the stresses. However, in packing and cushioning foams, precise tuning of this response is not possible due to randomness of the foam microstructure, and the lateral coupling among cells leading to strain localization, coordinated buckling and stiffness slope fluctuations. This is associated with the difficulty to fabricate perfectly periodic foams or honeycombs with specific microstructure geometry. To assess the applicability of χ-springs for use in these purposes, an ABAQUS simulation is constructed in which a "cushion" comprised of a row of parallel 1D line springs covered by an extensible 0.5 mm thick polyurethane sheet. This cushion is indented by a rigid body with several asperities (depicted in **Figure 5**a). Each spring depicted in Figure 5a represents χ-spring or, for benchmarking, a foam element with the same geometric

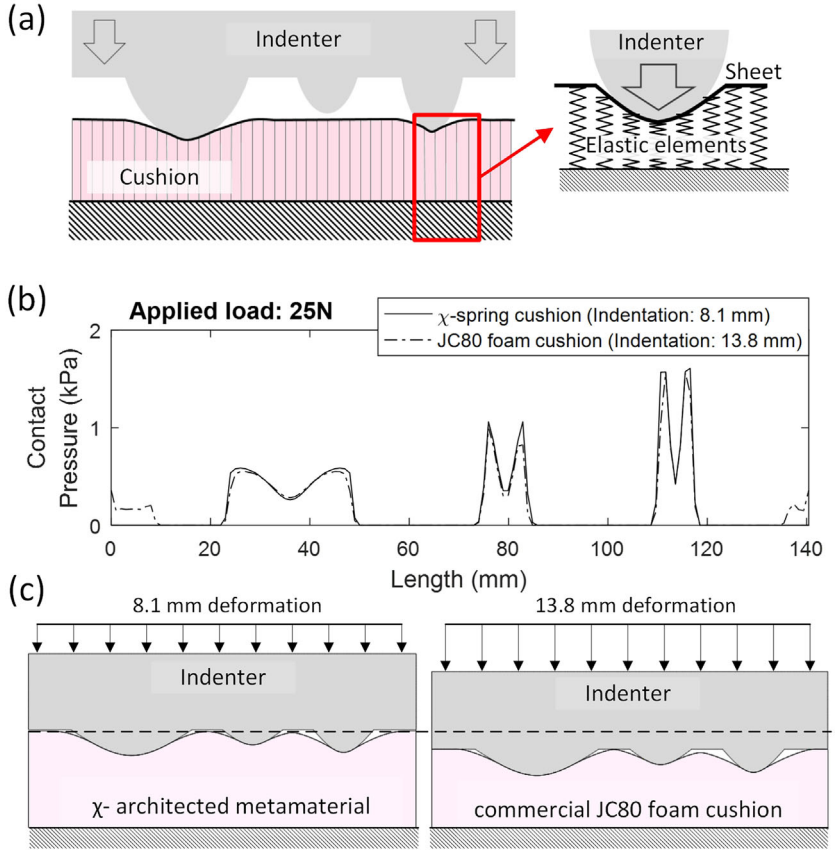

Figure 5. Architected metamaterials for stress re-distribution. a) Schematic showing an indenter with asperities penetrating a "cushion" of spring elements coupled by an extensible sheet. The springs represent either, χ-springs or an appropriately sized commercial JC80 foam element. b) Contact pressure distribution over the perimeter of the indenting surface for the different "springs" with an applied load of 25 N (more load cases can be found in the supplementary information). The equilibrium indentation is specified in the plot legend for each case. c) Snapshot of the ABAQUS simulation comparing indentation depths at 25 N applied load. Individual springs are not rendered. Dashed line indicates undeformed thickness of the cushion.

footprint. JC80 (Johnson Controls) light polyurethane foam is chosen as it is commonly used for cushioning applications.[29] Each of the spring elements is constrained to only be displaced in the vertical direction. The dimension of the system in the out of plane direction is set to be the width of each element (22 mm). Contact between the indenter and sheet is treated as frictionless contact as the χ-springs strain is constrained to the vertical direction.

An appropriate χ-spring architected metamaterial is chosen based on the parametric study in Figure 4. We choose, an element with $L = 14$ mm and $t = 2$ mm since it provides a suitable tradeoff between plateau width and strain energy stored. Normal contact pressure is applied in the form of loads of 7, 15, 25, 33, and 39 N on the indentor. For each load, the peak local stress and the maximum deformation at this stress is compared between the cases of the χ-spring and the JC80 foam cushions. For the small load (7, 15, and 25 N), the χ-springs offer lower deformation values without causing large contact pressure stress. This response can be visualized by observing normal contact pressure plotted along the perimeter length of the indenting surface for the applied load of 25 N (Figure 5b). For applied loads up to 33 N, the JC80 foam and χ-spring configuration elements have comparable peak contact pressure, meaning they can almost equally re-distribute stresses. However, the JC80 foam cushion deforms by 70.3% more than the χ-spring cushion. This shows the benefits of using χ-spring architected metamaterial compared to commercial JC80 foam. In particular, the properties of the χ-spring can be precisely tailored to accommodate this load and distribute the stresses exerted by non-uniform bodies while minimizing local deformation. This type of behavior can have strong implications in materials for cushioning, packaging, and energy absorption. It important to note that the spring dimensions are tailored for a specific load range. For loads higher than 33 N, the χ-spring metamaterial densifies more rapidly than the JC80 resulting in worse performance at those loads (see Supporting Information). This is expected as the thickness of each individual strut is much thicker $O(1\,\text{mm})$ than the cell walls of JC80 foam $O(0.01\,\text{mm})$[29]. Furthermore, the onset of densification (transition into regime III behavior) is smoother in the case of JC80 foam as new points of contact are established more gradually with increasing deformation due to the inherent variation between unit cells.

In summary, we present a class of materials, where the internal architecture exploits local buckling to achieve essential nonlinear stiffness. The material construction can be 2D (prismatic) which opens up opportunities for fabrication using laser cutter —as demonstrated in this manuscript- as well as simple molding, die cutting and lithography. The metamaterial exhibits a wide flat stress plateau —zero stiffness- followed by a stiffening regime, leading to what is known as essential stiffness nonlinearity. The proposed structures can be used as individual elements or as components of lattice materials. Two possible configurations, the τ- and the χ-springs are studied in detail and the phenomenon is shown experimentally to be robust for both these configurations over a range of geometrical parameters. Finite element models and simplified beam models are used to isolate the mechanisms of achieving flat stress plateau, and reveal that the essentially nonlinear behavior is a purely geometrical effect arising from by asymmetric buckling modes. Moreover, the structures are fully reversible when compressed — even to the point of densification. Such elements can be utilized in cushioning and packaging, where they offer the same ability for minimizing stress concentration at contact points yet achieve much smaller deformations. In the future, combining pairs of these elastic elements in pre-compressed states (such that the pre-compressed equilibrium is in regime II) can produce essentially nonlinear springs or even mimic vibro-impact

behavior and has applications in the design of acoustic metamaterials such as sonic vacua and acoustic non-reciprocity.

Supporting Information

Supporting information is available online from Wiley Online Library or from the author.

Acknowledgements

The authors acknowledged fruitful discussions with Professors Alexander Vakakis, Chiara Daraio and Michael Leamy. This study was supported by the NSF EFRI-NewLAW- 1741565.

Conflict of Interest

The authors declare no conflict of interest

Keywords

architected materials, buckling, cushioning, nonlinear materials, shock absorption

Received: July 19, 2018
Revised: September 6, 2018
Published online: October 11, 2018

[1] R. Lakes, *Science* **1987**, *235*, 1038.
[2] G. W. Milton, *J. Mech. Phys. Solids* **1992**, *40*, 1105.
[3] T. Bückmann, M. Thiel, M. Kadic, R. Schittny, M. Wegener, *Nat. Commun*. **2014**, *5*, 4130.
[4] M. Kadic, T. Bückmann, N. Stenger, M. Thiel, M. Wegener, *Appl. Phys. Lett*. **2012**, *100*, 191901.
[5] J. K. Raghunath, *Strongly Nonlinear Acoustics of One-Dimensional Granular Sonic Vacua*, University of Illinois at Urbana-Champaign, IL, USA **2013**.
[6] A. Rafsanjani, A. Akbarzadeh, D. Pasini, *Adv. Mater.* **2015**, *27*, 5931.
[7] D. M. Correa, T. Klatt, S. Cortes, M. Haberman, D. Kovar, C. Seepersad, *Rapid Prototyping J*. **2015**, *21*, 193.
[8] S. Shan, S. H. Kang, J. R. Raney, P. Wang, L. Fang, F. Candido, J. A. Lewis, K. Bertoldi, *Adv. Mater.* **2015**, *27*, 4296.
[9] D. Yang, L. Jin, R. V. Martinez, K. Bertoldi, G. M. Whitesides, Z. Suo, *Extreme Mech. Lett*. **2016**, *6*, 1.
[10] B. Florijn, C. Coulais, M. van Hecke, *Phys. Rev. Lett*. **2014**, *113*, 175503.
[11] P. Wang, F. Casadei, S. Shan, J. C. Weaver, K. Bertoldi, *Phys. Rev. Lett*. **2014**, *113*, 014301.
[12] J. Yang, Y. Xiong, J. Xing, *J. Sound Vib*. **2013**, *332*, 167.
[13] A. Carrella, M. Brennan, T. Waters, V. Lopes Jr, *Int. J. Mech. Sci*. **2012**, *55*, 22.
[14] I. Kovacic, M. J. Brennan, T. P. Waters, *J. Sound Vib*. **2008**, *315*, 700.
[15] X. Liu, X. Huang, H. Hua, *J. Sound Vib*. **2013**, *332*, 3359.
[16] A. Carrella, M. Brennan, T. Waters, *J. Sound Vib*. **2007**, *301*, 678.
[17] N. Zhou, K. Liu, *J. Sound Vib*. **2010**, *329*, 1254.
[18] K. J. Moore, J. Bunyan, S. Tawfick, O. V. Gendelman, S. Li, M. Leamy, A. F. Vakakis, *Phys. Rev. E* **2018**, *97*, 012219.
[19] J. Bunyan, K. J. Moore, A. Mojahed, M. D. Fronk, M. Leamy, S. Tawfick, A. F. Vakakis, *Phys. Rev. E* **2018**, *97*, 052211.
[20] H. Cho, M.-F. Yu, A. F. Vakakis, L. A. Bergman, D. M. McFarland, *Nano Lett*. **2010**, *10*, 1793.
[21] S. A. Hubbard, D. M. McFarland, L. A. Bergman, A. F. Vakakis, G. Andersen, *AIAA J*. **2014**, *52*, 2633.
[22] A. F. Vakakis, O. V. Gendelman, L. A. Bergman, D. M. McFarland, G. Kerschen, Y. S. Lee, *Nonlinear Targeted Energy Transfer in Mechanical and Structural Systems*, Vol. *156*, Springer Science & Business Media, Dordrecht, the Netherlands **2008**.
[23] V. M. Eguíluz, M. Ospeck, Y. Choe, A. Hudspeth, M. O. Magnasco, *Phys. Rev. Lett*. **2000**, *84*, 5232.
[24] P. Frantík, *Eng. Mech*. **2007**, *14*, 155.
[25] M. F. Ashby, R. M. Medalist, *Metall. Trans. A* **1983**, *14*, 1755.
[26] M. Ashby, *Philos. Trans. R. Soc. London A: Math. Phys. Eng. Sci*. **2006**, *364*, 15.
[27] L. J. Gibson, M. F. Ashby, *Cellular Solids: Structure and Properties*, Cambridge University Press, Cambridge, United Kingdom **1999**.
[28] D. Boal, D. H. Boal, *Mechanics of the Cell*, Cambridge University Press, Cambridge, United Kingdom **2012**.
[29] D. De Vries, *Characterization of Polymeric Foams*, Eindhoven University of Technology, Eindhoven, the Netherlands **2009**.

